JCI The Journal of Clinical Investigation

p38 mitogen-activated protein kinase regulates chamber specific perinatal growth in heart

Tomohiro Yokota, … , Susumu Minamisawa, Yibin Wang

J Clin Invest. 2020. https://doi.org/10.1172/JCI135859.

Research In-Press Preview Cardiology

Graphical abstract

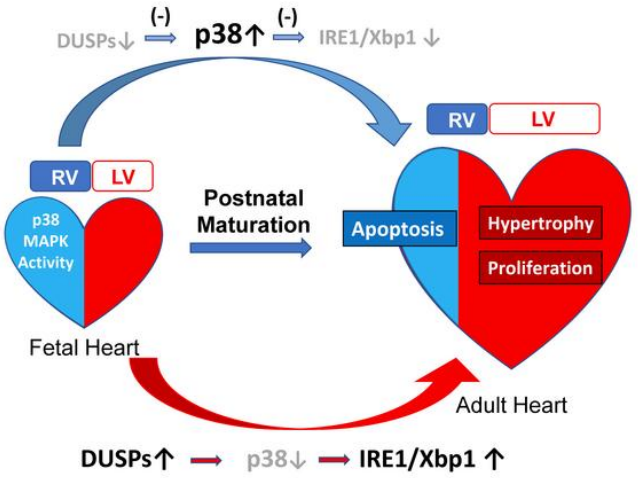

p38 MITOGEN-ACTIVATED PROTEIN KINASE REGULATES CHAMBER SPECIFIC PERINATAL GROWTH IN HEART

Tomohiro Yokota[1], Jin Li[1], Jijun Huang[1], Zhaojun Xiong[1, 2], Qing Zhang[3], Tracey Chan[3], Yichen Ding[4,5], Christoph Rau[1], Kevin Sung[4], Shuxun Ren[1], Rajan Kulkarni[4,6], Tzung Hsiai[4, 5], Xinshu Xiao[3], Marlin Touma[7], Susumu Minamisawa[8] and Yibin Wang[1,5]

*

1) Departments of Anesthesiology, Physiology and Medicine, Cardiovascular Research Laboratories, David Geffen School of Medicine, University of California, at Los Angeles Los Angeles, CA 90095, USA

2) Department of Cardiology, The 3rd Affiliated Hospital of Sun Yat-sen University, Guangzhou, China

3) Integrative Biology and Physiology, David Geffen School of Medicine, University of California at Los Angeles, Los Angeles, CA, USA.

4) Department of Bioengineering, School of Engineering and Applied Sciences, University of California, Los Angeles, CA 90095, USA

5) Division of Cardiology, Department of Medicine, David Geffen School of Medicine

at UCLA, Los Angeles, CA 90095, USA

6) Division of Dermatology, Department of Medicine, David Geffen School of Medicine at UCLA, Los Angeles, CA 90095, USA

7) Department of Pediatrics, David Gefen School of Medicine, University of California, at Los Angeles, CA 90095

8) Department of Cell Physiology, Jikei University, Tokyo, Japan.

*Corresponding Address:

Yibin Wang, Ph.D.

Department of Anesthesiology and Division of Molecular Medicine

Room BH 569 CHS, 650 Charles E. Young Drive, Box 957115

David Geffen School of Medicine, University of California at Los Angeles

Los Angeles, CA 90095

Email: yibinwang@mednet.ucla.edu

Tel: (310) 206-5197

Fax: (310) 206-5907

The authors have declared that no conflict of interest exists.

ABSTRACT

In mammalian heart, left ventricle (LV) rapidly becomes more dominant in size and function over right ventricle (RV) after birth. The molecular regulators responsible for this chamber specific differential growth are largely unknown. We found the cardiomyocytes in neonatal mouse RV had lower proliferation, more apoptosis and smaller sizes comparing to the LV. Such chamber specific growth pattern was associated with a selective activation of p38 MAPK activity in the RV and simultaneous inactivation in the LV. Cardiomyocyte-specific deletion of both *mapk14* and *mapk11* genes in mice results in loss of p38 MAP kinase expression and activity in the neonatal heart. Inactivation of p38 activity led to marked increase in myocytes proliferation and hypertrophy but diminished myocyte apoptosis, specifically in the RV. Consequently, the p38 inactivated hearts showed RV specific enlargement postnatally, progressing to pulmonary hypertension and right heart failure at adult stage. Chamber-specific p38 activity was associated with differential expression of dual-specific phosphatases (DUSPs) in neonatal hearts, including Dusp26. Unbiased transcriptome analysis revealed IRE1α/XBP mediated gene regulation contributed to p38 MAPK dependent regulation of

neonatal myocyte proliferation and binucleation. These findings establish an obligatory role of DUSP-p38-IRE1 signaling in myocytes for chamber specific growth in postnatal heart.

INTRODUCTION

In fetal mammalian heart, the right ventricle (RV) has the equivalent size comparing to the left ventricle (LV) and even more dominant over LV in terms of cardiac output when both chambers contribute to a common circulation. During the postnatal transition after birth, LV takes over RV quickly in terms of contractile function, chamber size and wall thickness. This differential growth is critical for the two ventricles to accommodate the dramatic changes in the circulatory system after birth, including separation of peripheral vs. pulmonary circulations, a significant increase in the peripheral resistance for the left ventricle and a simultaneous decrease in the pulmonary vascular resistance for the right ventricle (1).

The developmental origins of the left vs the right ventricle are different, with LV is derived from the first heart field while RV from the second heart field (2). The differential growth pattern observed between LV and RV during this postnatal transition period has largely been attributed to myocyte proliferation and hypertrophy, resulting in a significantly bigger LV vs. RV in adolescent and adult heart (3, 4). Much of our current understanding to this chamber-specific postnatal growth is based on a prevailing

paradigm that external factors such as intra-chamber pressure (or sheer stress), hormonal signals, vascular growth and sympathetic innervation dictate the chamber-specific postnatal growth (5, 6). However, the intracellular molecular mechanism and the signal network in cardiomyocytes responsible for the chamber-specific postnatal growth and remodeling are largely unknown.

p38 mitogen-activated protein kinases (MAPKs) belong to a branch of ser-thr protein kinases, with four family members encoded by genes *Mapk11*, *12, 13* and *14* for the isoforms β, γ, δ and α, respectively. p38 MAPKs are originally identified as stress-induced signaling molecules involved in a variety of cellular stress responses, including inflammation, oxidative injury, mechanical overload and hormone stimulation (7, 8). Extensive evidence from *in vivo* studies demonstrate a broad impact of p38 MAPK activity on infection, inflammation, tissue injury and repair (9). Moreover, recent genetic studies have also demonstrated an important role for specific p38 isoforms in cellular differentiation and growth in skin, muscle and bone (10-12). In mammalian heart, p38 activities are implicated in cardiomyocyte hypertrophy, inflammatory gene induction, cardiac fibrosis, myocyte apoptosis and suppression of neonatal myocyte

proliferation(13). Although p38 MAPK inhibition has been proposed as a potential therapeutic strategy to treat heart diseases (14, 15), cardiomyocyte specific knockout of p38α results in an exacerbated form of cardiomyopathy and pathological remodeling following pressure-overload in mice(16, 17), highlighting the complexity of p38 MAPK pathway in both cardiac physiology and pathogenesis of heart failure.

In an effort to uncover the intrinsic signaling mechanisms participating in the chamber-specific postnatal growth, we measured the activities of MAP kinases in neonatal mouse heart. Among the three major MAP kinase pathways, we found p38 MAPK activities were significantly and specifically induced in RV but diminished in LV during the first week after birth, while the other MAPK pathways including JNK and ERK were not altered. Genetic inactivation of p38 in the neonatal mouse hearts was achieved in a cardiac specific *mapk14/11* double knockout (p38-cdKO) mouse model. From histological, cellular and molecular analyses, we found that the p38-cdKO mice developed remarkable RV-specific chamber enlargement and dilation, which was associated with a significant increase in RV myocyte proliferation and hypertrophy, and a reduction of apoptosis while postnatal growth of LV was largely unaffected. We further

demonstrated that differential expression of dual-specific phosphatases (DUSP), including DUSP26, was correlated with chamber specific p38 MAPK activities in the neonatal myocytes. Furthermore, an unexpected IRE1a/Xbp1 dependent signaling was involved in p38 MAPK dependent regulation of cell cycle gene regulation, myocyte proliferation and binucleation. Thus, our study has revealed a previously uncharacterized molecular and signaling network necessary for chamber specific post-natal remodeling and growth in neonatal mouse heart.

RESULTS

Chamber-specific activation of p38 MAP kinase during postnatal heart development

In neonatal mouse hearts, we observed a dramatic growth in chamber sizes soon after birth but at different rates between the left (LV) and the right (RV) ventricles (**Figure 1A**). This was associated with a higher level of myocyte proliferation in LV vs. RV as demonstrated by the number of phospho-histone 3 (pH3) positive myocytes and total myocyte numbers in the LV. In addition, cardiomyocytes in LV had bigger sizes while RV showed a transient induction of TUNEL positive myocytes (**Figure 1 B-E**). Because MAPKs are known to be involved in the cellular processes of hypertrophy, proliferation and programmed cell death, we measured the activation status of all three major branches of MAPKs in neonatal hearts, including ERK1/2, p38 and JNK **(Figure 1 F-K)** using free wall tissues from LV and RV**.** The chamber origins of the collected tissue were demarcated by the differential expression of Hand1 (for LV) and Hand2 (for RV) (**Figure 1L**). The activation states of ERK and JNK, as indicated by the phosphorylated vs the total protein levels, were not changed during perinatal development nor differentially regulated between LV and RV. In contrast, p38 MAPK showed significant activities in the RV tissue from neonatal hearts during P1 to P7 period while its activities in the LV

remained inactivated below detection limit throughout the neonatal period. This chamber-specific activation profile of p38 MAPK raised the question about its role in the chamber-specific growth pattern in perinatal hearts.

RV-specific abnormality in the cardiac-specific p38 MAP kinases knockout mice

To examine the functional role of p38 MAPK activity in neonatal heart, we generated a mouse model (p38-cdKO) with cardiac specific deletion of both p38α (encoded by *mapk14*) and p38β genes (encoded by *mapk11*) using MLC2a-Cre (18) mediated genomic DNA deletion as described in the Methods. Near complete loss of p38 protein expression in the LV and the RV tissues was observed from the p38cdKO hearts, demonstrating the effectiveness of targeted gene inactivation (**Figure S1A and S1B**). Among the offspring, the genotype distribution showed an expected ratio of 50%:50% between the Control ($mapk11^{fl/fl}mapk14^{fl/fl}$) and the p38-cdKO ($mapk11^{fl/fl}mapk14^{fl/fl}$*mlc2a-cre*) during fetal development, but was reduced to 21%, 35%, 27% and 26% at P0, P1, P3 and P7 respectively (**Table S1**), suggesting premature death in the perinatal period. The survived p38cdKO mice showed an abnormal gross

morphology in the heart (**Figure 2A and 2B**). Three-dimensional light-sheet microscopy revealed an enlargement of RV in the p38cdKO hearts comparing with the Control (**Figure 2C-F, Movie S1-4**). Histological analysis confirmed an increase in RV wall thickness and chamber dimension in the p38 cdKO hearts comparing to their littermate Controls at day P1, P7 (**Figure 2G-2J**) and beyond (**Figure S1C**). Consistent with these histological observations, the right ventricle weight and the right atrium weight were significantly higher in the p38cdKO hearts comparing to the Controls, starting from P1 onward but not in the E19.5 fetal hearts (**Figure 2K-M)**. Remarkably, the p38cdKO mice showed normal body weight, as well as normal left ventricle, left atrium, and lung weights during the same perinatal period (**Figure 2N-Q**). There were no differences in fibrotic area within myocardium between the two genotype groups at P7 and 1-month age, and neither any changes between the two chambers (**Figure S1D and S1E**). Therefore, p38 MAPKs activity is differentially activated in the peri-natal RV and cardiomyocyte specific inactivation of p38 MAPKs in neonatal mouse hearts leads to RV specific enlargement without signs of LV or pulmonary abnormalities.

We also analyzed the dynamic progression of cardiac remodeling in intact mouse

hearts based on serial echocardiographic assessment in the postnatal period. To measure wall thickness and inner diameter of LV and RV, we used an M-mode in cross-sectional direction as illustrated in **Figure S1F** and **S1G,** in order to measure both LV and RV simultaneously. The p38 cdKO mice showed normal RV wall thickness at P1 but increased significantly from P3 onward (**Figure 3A**) comparing to the Controls while a significant increase in the RV inner diameter was detected starting at P1, indicating an abnormal growth in both thickness and diameter of RV in the p38-cdKO heart (**Figure 3B**). There was no change in pulmonary artery velocity at P1 and P3 in the p38-cdKO mice, however, a modest but significant increase in pulmonary artery velocity was observed starting from P7 and progressively elevated beyond the postnatal period for up to 8 months in adult hearts, indicating that pulmonary hypertension was developed secondary to RV remodeling (**Figure 3C**). Due to the abnormal RV growth, LV chamber in the p38cdKO mice was compressed but showed no signs of hypertrophy or dysfunction (**Figure 3D-F**). In contrast, a persistent elevation of pulmonary acceleration time was observed, consistent with a state of pulmonary hypertension. However, there were no changes in the pulmonary ejection time in the p38-cdKO hearts up to 8 months of age

(**Figure 3G-I**). RV weight increased nearly two folds at 4 and 8 months of age in the p38-cdKO heart vs. the Control, in contrast, no differences were observed in the LV weight between the two genotypes across all time points (**Figure 3J and 3K**). Finally, lung weight significantly increased in the p38-cdKO mouse only after 4 and 8 months of age (**Figure3L).** All these data suggested that abnormal RV growth was a primary outcome from p38 inactivation, and pulmonary hypertension was likely a secondary effect. In summary, we establish that cardiomyocyte specific p38 inactivation leads to RV specific abnormalities at both morphological and functional levels in the neonatal mouse heart.

p38 MAPK inactivation specifically prolongs cardiomyocyte proliferation in post-natal right ventricle

By immunofluorescent staining, the number of phosphor-histone 3 (pH3) positive cardiomyocytes increased significantly in RV of the p38 cdKO hearts comparing to the Controls throughout the entire perinatal period, while no significant difference was observed in LV (**Figure 4A-C**). In addition, the total number of myocytes was significantly higher in RV of the p38cdKO comparing to the Controls at P3 and P7 while

no change was detected in LV (**Figure 4D and 4E**). Consistent with the observed increase of myocyte proliferation, the expression of several cell cycle inhibitory genes, including p21, Wee1, and Rb, was reduced specifically in the RV of p38 cdKO hearts comparing to the Controls whereas no significant differences were detected in LV (**Figure 4F-I**). Phosphorylated Rb vs. total Rb ratio was also increased specifically in the p38cdKO right ventricle at all time points (**Figure 4J**). We also examined other signaling molecules previously implicated in cardiomyocytes proliferation regulation, including Yap (19-21) and Gsk3β (22). They were not affected in either chambers by the p38 inactivation (**Figure S2A-C**). All of these data suggest that RV-specific p38 activation is a necessary signal to modulate cardiomyocyte proliferation in the right ventricle during normal postnatal development. However, p38 mediated regulation of cardiomyocyte proliferation in RV does not appear to involve Hippo or GSK3β pathways.

p38 MAPK inactivation reduces right ventricle myocyte apoptosis in the neonatal heart

As shown in **Figure 1** and an earlier study in rat (3), RV-specific induction of

cardiomyocyte apoptosis may also contribute to chamber-specific differential growth in the postnatal heart. Using TUNEL assay, we found that the transient induction of cardiomyocyte apoptosis at P1 time point was significantly blunted in RV by p38 inactivation, whereas no change was observed in LV (**Figure 5A-C, Figure S3A-B)**. Associated with the loss of apoptotic signal, the expression of anti-apoptotic protein Bcl2 was increased in the RV at P1 time point in the p38cdKO hearts (**Figure 5D**).

p38 MAPK inactivation induces cardiomyocyte hypertrophy specifically in the neonatal right ventricle

By cross-section area measurements, myocytes in RV showed a significant enlargement in cell sizes from P1 to 1 month of age comparing to the Controls (**Figure 5E-J, 5M, and Figure S3C-F**). On the other hand, the LV myocytes showed no differences in sizes between the p38cdKO and the Control hearts (**Figure 5K, 5L, 5N, and Figure S3G-N**). These results suggest that RV specific p38 activation during postnatal stage is necessary to modulate RV cardiomyocyte hypertrophy in the postnatal hearts.

p38 MAPK and chamber-specific transcriptome programming in neonatal mouse heart

To uncover the underlying molecular mechanism in RV specific p38 activation and p38 dependent neonatal heart remodeling, we examined the expression of known upstream regulators of p38 MAPK activities, including MKK3, MKK3 phosphorylation, TAB1 and Cdc37 by immunoblot, and detected no differences between LV and RV (data not shown). To explore further, we conducted transcriptome analysis by RNA-seq using tissues from left and right ventricular free-wall of P1 and P3 p38cdKO hearts and the corresponding tissues from the Control hearts. Using >1.2 fold and $p<0.05$ as selection criteria, we detected 2,242 and 1,789 genes differentially expressed in RV between the p38 cdKO and the Control at P1 and P3, respectively. On the other hand, 2,823 and 1,455 genes (same FC>1.2 fold and $p<0.05$ threshold) were differentially expressed in LV from the same cohorts (**Table S2-5**). We performed Principal Component Analysis (PCA) for all the detected genes (**Figure 6A**). Withstanding the limitation of the PCA analysis, based on the two dimensions with the highest contributions to the variations, we observed a remarkable separation of global gene expression profiles between the left and the right

ventricle from P1 to P3 in the Control mice, indicating that chamber specific molecular identity was rapidly established after birth in new born mouse hearts (**Figure 6A**). In contrast, the p38cdKO heart showed marked shift in global gene expression from their wildtype counterparts, and LV and RV transcriptome from the p38cdKO hearts had extensive overlap at P3 (**Figure 6A).** Therefore, cardiomyocyte specific p38 MAPK inactivation led to global changes in gene expression in the postnatal hearts, leading to diminished chamber specificity at transcriptome level.

Based on GO classification for the up-regulated genes detected in the p38 cdKO hearts, we found that cell-cycle related processes were ranked at the top in RV at both P1 and P3 time points (**Figure 6B-C,** highlighted by brackets), whereas similar functional enrichment was identified in the LV only at P1 but not P3 time point (**Figure S4A -B**). Furthermore, GO analysis for the down-regulated genes in the p38 cdKO heart revealed a significant enrichment for apoptosis in RV at P1 time point (**Figure 6D-E,** highlighted by an arrow), whereas no such signal was detected in LV (**Figure S4C-D**). Further analysis of the DEGs revealed a significant overlap between LV and RV in the genes affected by p38 inactivation **(Figure 6F)**. The vast majority of the genes affected by p38

inactivation showed modest fold of changes (**Figure S4E**, **Figure 6G**). While the cell cycle related genes were ranked at the top based on fold of changes in both left and right ventricles, the magnitudes of p38 dependent gene expression changes were much higher in the RV than in the LV (**Figure 6H).** This was consistent with the differential p38 activities observed in the two chambers, further supporting that cell-cycle regulation in the neonatal heart were p38 activity dependent. Among the differentially expressed genes between LV and RV, there were several known dual-specific phosphatases which could target p38 (**Table S6**). In particular, Dual-Specificity Protein Phosphatases 26 (Dusp26) showed a higher expression in RV vs. LV at both P3 and P7 time points as validated by RT-PCR (**Figure 7A**). To test if differential expression of Dusp26 contributed to p38 kinase mediated signaling, we knocked down Dusp26 in rat neonatal ventricular myocytes (NRVM) (**Figure S4F**), which indeed led to a significant activation of p38 activity in the NRVM (**Figure 7B**). Interestingly, Dusp26 inactivation also enhanced the expression of a number of RV-enriched genes but reduced the expression of a number of LV enriched genes (**Figure 7C**), supporting its regulatory role in chamber specificity. Furthermore, Dusp26 inhibition reduced the basal proliferative activity of NRVM and

this effect was completed blunted by p38 MAPK inhibition (**Figure 7D**), suggesting again that LV specific p38 inactivation is a downstream event of Dusp26 and Dusp26-p38 signaling contributes to chamber specific neonatal myocyte proliferation.

Xbp1 is a downstream molecule mediating p38 MAPK regulated cardiomyocyte proliferation

In order to establish the molecular basis for the observed p38 dependent regulation of cell-cycle related genes, we performed whole genome rVISTA analysis for the genes affected by p38 inactivation. A number of transcription factors were identified as potential upstream regulators in RV at P1 or P3, including E2F which was a well-established master regulator of cell cycle regulation (**Figure 8A**). Unexpected, however, we also found Xbp1, an ER stress response factor, among the top candidate transcription factors for the p38 regulated genes in RV at both P1 and P3 time points and in LV at P1 (**Figure 8A and S5**).

IRE1α/Xbp1 in the regulation of neonatal cardiomyocyte proliferation

To validate if Xbp1 activity was indeed related to p38 mediated regulation in

neonatal hearts, we examined and found the expression of IRE1α, an upstream activator of Xbp1 (23), was also significantly up-regulated in the p38 cdKO right ventricles (**Figure 8B**) while a parallel ER stress regulator ATF6 expression was not affected by p38 inactivation in RV (**Figure S6A-B**). In the Dusp26 knockdown cardiomyocytes, IRE1α expression was also significantly reduced (**Figure 7C**). During ER stress, IRE1 mediated Xbp1 mRNA splicing results in the production of nucleus localized sXbp1 protein for downstream gene expression(24, 25). sXbp1 was detected to at lower level in RV than in LV in the Control neonatal hearts, correlating well with the differential p38 activities between the two chambers. However, sXbp1 was significantly up-regulated only in the RV of the p38cdKO hearts **(Figure 8C**), with a concurrent reduction of the cytoplasmic sXbp1 (**Figure S6C)**. These data indicate that p38 MAPK inactivation induces Xbp1 activity via an IREα mediated post-transcriptional splicing and nuclei translocation.

To directly demonstrate the cell-autonomous effect of p38 activity on IRE1α/Xbp1 signaling, we treated NRVM with a p38 MAPK specific inhibitor SB202190 (10μM), which led to a significant induction of IRE1α expression (**Figure 8D).** As expected, the ratio between the spliced active sXbp1 vs. the un-spliced inactive

Xbp1 (uXbp1) was also induced following p38 MAPK inhibition, similar to what was observed in the p38cdKO heart (**Figure 8E)**. Furthermore, we found that ectopic expression of IRE1α in NRVM was sufficient to enhance myocyte proliferation in the same manner as p38 inhibition (**Figure 9A-B, S6D**). Interestingly, the presence of binucleated myocytes, a sign of myocyte growth and maturation, was also induced in the neonatal myocytes treated with either p38 inhibitor or IRE1α expression(**Figure 9C**).

Finally, we inactivated Xbp1 expression using an siRNA (siXbp1) and simultaneously inhibited p38 activity using SB202190 in NRVMs (**Figure S6E**). Xbp1 inactivation significantly blunted p38 inhibition-induced NRVM proliferation (**Figure 9D-E, and S6F).** A cell cycle regulatory gene, Ccnb2 (CyclinB2), was identified as a Xbp1 regulated gene based on rVISTA analysis (**Figure S6G**), and its expression was upregulated by p38 inhibition and this induction was also blunted by Xbp1 inactivation (**Figure 9F**). Notably, IRE1α/Xbp1 signaling had no effect on neonatal myocyte hypertrophy (**Figure S6H and S6I**). Taken together, these *in vivo* and *in vitro* data suggest that IRE1α/Xbp1 signaling is a previously uncharacterized downstream target of p38 activity in neonatal cardiomyocytes, contributing to p38 mediated chamber specific

regulation of myocyte proliferation and binucleation. (26-30)

DISCUSSION

In this report, we have uncovered an intrinsic cellular signaling in RV specific postnatal growth. We find that p38 MAPKs activity is selectively and dynamically induced in a RV-specific manner associated with lower levels of cardiomyocyte hypertrophy, proliferation and a higher level of apoptosis in RV than LV in perinatal mouse hearts. Cardiac-specific inactivation of p38 α/β isoforms led to RV-specific enlargement in postnatal hearts, likely contributed by elevated proliferation and hypertrophy concomitant with reduced apoptosis in RV. Mechanistically, we establish the IRE1α/Xbp1 signaling is a previously uncharacterized downstream signaling of p38 MAPK, which contributes to cardiomyocyte proliferation. Therefore, our study has revealed an unexpected role for two interconnected stress-response pathways, p38 MAPK and IRE1/Xbp1, in the regulation of chamber specific myocyte proliferation during normal perinatal transition. To our knowledge, this is the first myocyte intrinsic signaling pathway identified in postnatal chamber-specific remodeling.

Chamber specific activation of p38 MAPK in RV during neonatal development is one of the key findings of this study. While p38 MAPK activity is elevated in the RV

at P1, P3 and P7, its activity is diminished below detectable levels in LV at the same perinatal time points. Despite the dramatic changes in hemodynamics, oxygen and hormone environment during this transition period, other parallel branches of MAPKs, i.e. ERK and JNK, are not altered. This level of specificity raises question about the involvement of hormones or mechanical stress in the observed differential p38 activation between the two chambers, as those external factors often affect all branches of the MAPK pathway (31). This is also consistent with the notion that canonical upstream kinases (MKK3 and MKK6) for p38 do not show differential activation pattern in the perinatal left vs. right ventricle. Although the complete molecular basis for the chamber specificity remains to be determined, it is plausible that myocyte intrinsic signaling network, such as differential expression of Dusp26, contributes to the chamber specific p38 activation. More investigation will be needed to determine myocyte cell-autonomous mechanism vs. environmental factors in p38 activation *in vivo*. In this study, the chamber specific activation of p38 was observed in the ventricles, however, their activities and role in left vs. right atria will still need to be established.

Dusp26 possesses potent phosphatase activity to dephosphorylate and inactivate

p38 MAPK while has little effect on the other MAPKs, ERK1/2 and JNK (32). Our data indicates that the LV-enriched expression of this protein phosphatase may contribute to the chamber specific inactivation of p38 MAPK in LV during postnatal heart development. However, we cannot exclude other protein phosphatases or p38 modulators can also potentially contribute to RV vs. LV -specific p38 activation in perinatal heart.

In this study, we provided extensive evidence that RV specific p38 MAPK activity is a necessary signaling event to regulate cardiomyocyte proliferation, hypertrophy and apoptosis. However, our understanding to the downstream events responsible for each of these cellular processes is incomplete. Based on the evidence obtained from the p38 cdKO hearts, we conclude that AKT pathway may not be involved in this process which contradicts an earlier report linking AKT with p38 activation in neonatal myocyte proliferation regulation (33), In contrast, we observed an upregulation of several other growth factors in the p38 cdKO RV, including TGF-β2, Insulin growth factor, and Neuregulin1 (Nrg1). Each of them, especially Nrg1, is known to play a role in chamber morphogenesis and cardiomyocyte proliferation regulation (34-38). Bmp10 was also up-regulated in the p38cdKO RV. Both Nrg1 and Bmp10 are essential for the

chamber formation during fetal development(37). Therefore, p38 MAPK may regulate RV-specific myocyte proliferation and growth via several downstream growth signal molecules and morphogens. However, their specific contribution to the p38 mediated chamber-specific postnatal growth still needs to be experimentally demonstrated. In addition to the apparent impact on myocyte proliferation, the *in vitro* evidence also indicates that p38 activity affects neonatal cardiomyocyte binucleation. Binucleation is a part of the maturation process in the neonatal mammalian hearts. It is interesting to note that a recent systems based study finds that a cardiac specific MAP kinase Tnni3k is a key regulator of neonatal myocyte ploidity (39). Tnni3k is also an upstream regulator of p38 MAP kinase involved in cardiac injury and pathological remodeling in the adult heart (40, 41). Therefore, the specific contribution of Tnni3K in p38 dependent effect on myocyte binucleation to the RV specific remodeling remains to be demonstrated *in vivo*.

Based on unbiased transcriptome profiling, we find that Xbp1 is also a potential transcription factor with a significant contribution to p38 MAPK dependent gene regulation. Indeed, the IRE1α/sXbp1 was selectively up-regulated in the p38-cdKO hearts *in vivo* as well as in the p38 inactivated neonatal myocytes *in vitro.* In addition,

IRE1α expression in myocytes was sufficient to promote cell proliferation, and p38 inhibition-induced NRVM proliferation was blunted by Xbp1 inactivation. These results suggest that IRE1/Xbp1 signaling is both necessary and sufficient for p38-dependent neonatal myocyte proliferation. The IRE1α/sXbp1 signaling is also known to regulate proliferation in cancer cells and pancreatic β-cells (42-44). It has a pro-survival role under various conditions(45, 46). Interestingly, a recent report by Wang *et al.* demonstrates that sXbp1 has a protective effect under ischemia/reperfusion in heart through the coupling of the unfolded protein response to the hexosamine biosynthetic pathway (47), suggesting that IRE1α/sXbp1 could also be involved in the regulation of myocyte apoptosis in neonatal hearts. In short, while p38 mediated signaling appears to be essential for all three aspects of cellular processes associated with differential development between LV vs. RV, i.e. myocyte proliferation, hypertrophy and apoptosis, the specific downstream mechanisms may be different for each process. Indeed, the molecular basis for p38 dependent regulation of IRE1a/Xbp1 activity remains entirely unclear and should be further elucidated. In addition, IRE1a/Xbp1 is identified as a novel downstream signaling axis based largely on *in vitro* evidence, more studies will be needed

to establish its contribution *in vivo.* In particular, it needs to be further demonstrated whether this pathway is a chamber specific myocyte-autonomous signaling or a mediator of yet-to-be identified external factor(s) that dictate chamber specific remodeling in the postnatal hearts.

Chamber specific remodeling is critical to postnatal cardiac physiology. It is intriguing to note that loss of p38 mediated signaling in neonatal myocytes led to approximately 25% mortality in neonates. However, despite of a significant elevation of pulmonary pressure due to enlarged right ventricle, the survived p38-cdKO mice appear to remain viable with no signs of left ventricle failure up to 8 months. The longer-term impact of such abnormality on cardiac output and viability will still need to be investigated. Nevertheless, the newly uncovered physiological role of p38/IRE1α/Xbp1 signaling in RV-specific postnatal development may also have implications in the pathogenesis of congenital heart disease where genetic predisposition and postnatal pathological stress may interfere normal myocyte proliferation, growth and survival in a chamber specific fashion.

METHODS:

The raw data, analytic methods, and study materials are described in full as on-line supplemental information. The genetic engineered mice and expression plasmids are available from Dr. Yibin Wang's lab at UCLA. The list of the differentially expression genes are included in the supplemental tables (On-line Supplemental Table 2 to 7). The entire RNA-seq dataset is deposited at NIH-SRA under accession number PRJNA639143. Information of antibodies utilized in this report is listed in the On-line Supplemental Table 8.

Animals

The cardiac specific p38 MAPK α (*mapk14*) and β (*mapk11*) knockout mice were generated by crossing *mapk14* loxP and *mapk11* loxP mice with myosin light chain 2a (MLC2a)-cre mice as previously reported (18, 33).The MLC2a-cre mice have the Cre cDNA knocked-in the mlc-2a locus and develop no cardiac phenotype as reported in several earlier studies (18, 48), (49). Although the endogenous MLC-2a gene expression is restricted in the atrial myocytes in the adult heart, its expression is distributed in all

chambers of the embryonic hearts, leading to efficient p38 KO in all ventricular myocytes. Age and sex matched littermates with homozygous *mapk14* loxP and *mapk11* loxP alleles but no MLC2a-cre allele were used as the Controls in this study.

Study Approval

All animal handling and procedures were carried out in compliance with UCLA guidelines and approved by UCLA IACUC.

Statistical Analysis

Data were indicated as mean ± SEM. Statistical analysis was performed using 2-tailed Student's unpaired t-test between two groups or one-way ANOVA with multiple comparisons test (Tukey) among multiple groups. P values <0.05 were considered statistically significant.

Supplemental Information

Supplemental Information, including Supplemental Experimental Procedures and 6 Supplemental Figures, 8 Tables, and 4 movies can be found online.

AUTHOR CONTRIBUTIONS:

TY and YW designed all experiments. TY, JH and JL performed all molecular and animal experiments, data analysis, data interpretation, and manuscript preparation. YW managed funding and contributed experimental design, data interpretation, and manuscript preparation. QZ, TC, CR, MT and XX contributed RNA-seq data analysis. YD, KS, TH, RK contributed the light-sheet imaging. VR contributed animal analysis. SM contributed data interpretation and manuscript preparation.

ACKNOWLEDGMENTS

This work was supported in part by grants from National Institute of Health, USA (HL070079, HL103205, HL108186 and HL110667) and DoD/ DOD/DHP PRMRP-IIRA (PR171540) for YW; TY was supported by Construction of Lab-exchange Type Health & Biomedical Science Research Consortium, Japan. Authors wish to thank Ms. Haiying Pu for excellent technical assistance in this study.

REFERENCES

1. Gill AW. Postnatal cardiovascular adaptation. *Arch Dis Child Fetal Neonatal Ed.* 2018.

2. Kelly RG. The second heart field. *Curr Top Dev Biol.* 2012;100:33-65.

3. Fernandez E, Siddiquee Z, and Shohet RV. Apoptosis and proliferation in the neonatal murine heart. *Dev Dyn.* 2001;221(3):302-10.

4. Smolich JJ, Walker AM, Campbell GR, and Adamson TM. Left and right ventricular myocardial morphometry in fetal, neonatal, and adult sheep. *Am J Physiol.* 1989;257(1 Pt 2):H1-9.

5. Bishop SP. The myocardial cell: normal growth, cardiac hypertrophy and response to injury. *Toxicol Pathol.* 1990;18(4 Pt 1):438-53.

6. Tucker DC, and Bishop SP. Use of embryonic heart grafted in oculo to assess neurohumoral controls of cardiac development. *Toxicol Pathol.* 1990;18(4 Pt 1):531-40.

7. Kim EK, and Choi EJ. Pathological roles of MAPK signaling pathways in human diseases. *Biochim Biophys Acta.* 2010;1802(4):396-405.

8. Kyriakis JM, and Avruch J. Mammalian mitogen-activated protein kinase signal transduction pathways activated by stress and inflammation. *Physiol Rev.* 2001;81(2):807-69.

9. Lee JC, Kumar S, Griswold DE, Underwood DC, Votta BJ, and Adams JL. Inhibition of p38 MAP kinase as a therapeutic strategy. *Immunopharmacology.* 2000;47(2-3):185-201.

10. Rodriguez-Carballo E, Gamez B, and Ventura F. p38 MAPK Signaling in Osteoblast Differentiation. *Front Cell Dev Biol.* 2016;4:40.

11. Efimova T. p38delta mitogen-activated protein kinase regulates skin homeostasis and tumorigenesis. *Cell Cycle.* 2010;9(3):498-05.

12. Keren A, Tamir Y, and Bengal E. The p38 MAPK signaling pathway: a major regulator of skeletal muscle development. *Mol Cell Endocrinol.* 2006;252(1-2):224-30.

13. Yokota T, and Wang Y. p38 MAP kinases in the heart. *Gene.* 2016;575(2 Pt 2):369-76.

14. Denise Martin E, De Nicola GF, and Marber MS. New therapeutic targets in

cardiology: p38 alpha mitogen-activated protein kinase for ischemic heart disease. *Circulation.* 2012;126(3):357-68.

15. Marber MS, Molkentin JD, and Force T. Developing small molecules to inhibit kinases unkind to the heart: p38 MAPK as a case in point. *Drug Discov Today Dis Mech.* 2010;7(2):e123-e7.

16. Nishida K, Yamaguchi O, Hirotani S, Hikoso S, Higuchi Y, Watanabe T, et al. p38alpha mitogen-activated protein kinase plays a critical role in cardiomyocyte survival but not in cardiac hypertrophic growth in response to pressure overload. *Mol Cell Biol.* 2004;24(24):10611-20.

17. Rose BA, Yokota T, Chintalgattu V, Ren S, Iruela-Arispe L, Khakoo AY, et al. Cardiac myocyte p38α kinase regulates angiogenesis via myocyte-endothelial cell cross-talk during stress-induced remodeling in the heart. *J Biol Chem.* 2017;292(31):12787-800.

18. Peng X, Wu X, Druso JE, Wei H, Park AY, Kraus MS, et al. Cardiac developmental defects and eccentric right ventricular hypertrophy in cardiomyocyte focal adhesion kinase (FAK) conditional knockout mice. *Proc Natl*

Acad Sci U S A. 2008;105(18):6638-43.

19. Xin M, Kim Y, Sutherland LB, Murakami M, Qi X, McAnally J, et al. Hippo pathway effector Yap promotes cardiac regeneration. *Proc Natl Acad Sci U S A.* 2013;110(34):13839-44.

20. Lin Z, and Pu WT. Releasing YAP from an alpha-catenin trap increases cardiomyocyte proliferation. *Circ Res.* 2015;116(1):9-11.

21. Morikawa Y, Heallen T, Leach J, Xiao Y, and Martin JF. Dystrophin-glycoprotein complex sequesters Yap to inhibit cardiomyocyte proliferation. *Nature.* 2017;547(7662):227-31.

22. Kerkela R, Kockeritz L, Macaulay K, Zhou J, Doble BW, Beahm C, et al. Deletion of GSK-3beta in mice leads to hypertrophic cardiomyopathy secondary to cardiomyoblast hyperproliferation. *J Clin Invest.* 2008;118(11):3609-18.

23. Calfon M, Zeng H, Urano F, Till JH, Hubbard SR, Harding HP, et al. IRE1 couples endoplasmic reticulum load to secretory capacity by processing the XBP-1 mRNA. *Nature.* 2002;415(6867):92-6.

24. Yoshida H, Oku M, Suzuki M, and Mori K. pXBP1(U) encoded in XBP1 pre-

mRNA negatively regulates unfolded protein response activator pXBP1(S) in mammalian ER stress response. *J Cell Biol.* 2006;172(4):565-75.

25. Yoshida H, Matsui T, Yamamoto A, Okada T, and Mori K. XBP1 mRNA is induced by ATF6 and spliced by IRE1 in response to ER stress to produce a highly active transcription factor. *Cell.* 2001;107(7):881-91.

26. Walsh S, Ponten A, Fleischmann BK, and Jovinge S. Cardiomyocyte cell cycle control and growth estimation in vivo--an analysis based on cardiomyocyte nuclei. *Cardiovasc Res.* 2010;86(3):365-73.

27. Leone M, Magadum A, and Engel FB. Cardiomyocyte proliferation in cardiac development and regeneration: a guide to methodologies and interpretations. *Am J Physiol Heart Circ Physiol.* 2015;309(8):H1237-50.

28. Matsuyama D, and Kawahara K. Oxidative stress-induced formation of a positive-feedback loop for the sustained activation of p38 MAPK leading to the loss of cell division in cardiomyocytes soon after birth. *Basic Res Cardiol.* 2011;106(5):815-28.

29. Shozawa T, Okada E, Kawamura K, Sageshima M, and Masuda H. Development

of binucleated myocytes in normal and hypertrophied human hearts. *Am J Cardiovasc Pathol.* 1990;3(1):27-36.

30. Soonpaa MH, Kim KK, Pajak L, Franklin M, and Field LJ. Cardiomyocyte DNA synthesis and binucleation during murine development. *Am J Physiol.* 1996;271(5 Pt 2):H2183-9.

31. Rose BA, Force T, and Wang Y. Mitogen-activated protein kinase signaling in the heart: angels versus demons in a heart-breaking tale. *Physiol Rev.* 2010;90(4):1507-46.

32. Yu W, Imoto I, Inoue J, Onda M, Emi M, and Inazawa J. A novel amplification target, DUSP26, promotes anaplastic thyroid cancer cell growth by inhibiting p38 MAPK activity. *Oncogene.* 2007;26(8):1178-87.

33. Engel FB, Schebesta M, Duong MT, Lu G, Ren S, Madwed JB, et al. p38 MAP kinase inhibition enables proliferation of adult mammalian cardiomyocytes. *Genes Dev.* 2005;19(10):1175-87.

34. Gemberling M, Karra R, Dickson AL, and Poss KD. Nrg1 is an injury-induced cardiomyocyte mitogen for the endogenous heart regeneration program in

zebrafish. *Elife.* 2015;4.

35. Baliga RR, Pimental DR, Zhao YY, Simmons WW, Marchionni MA, Sawyer DB, et al. NRG-1-induced cardiomyocyte hypertrophy. Role of PI-3-kinase, p70(S6K), and MEK-MAPK-RSK. *Am J Physiol.* 1999;277(5 Pt 2):H2026-37.

36. Hertig CM, Kubalak SW, Wang Y, and Chien KR. Synergistic roles of neuregulin-1 and insulin-like growth factor-I in activation of the phosphatidylinositol 3-kinase pathway and cardiac chamber morphogenesis. *J Biol Chem.* 1999;274(52):37362-9.

37. Grego-Bessa J, Luna-Zurita L, del Monte G, Bolos V, Melgar P, Arandilla A, et al. Notch signaling is essential for ventricular chamber development. *Dev Cell.* 2007;12(3):415-29.

38. D'Uva G, Aharonov A, Lauriola M, Kain D, Yahalom-Ronen Y, Carvalho S, et al. ERBB2 triggers mammalian heart regeneration by promoting cardiomyocyte dedifferentiation and proliferation. *Nat Cell Biol.* 2015;17(5):627-38.

39. Patterson M, Barske L, Van Handel B, Rau CD, Gan P, Sharma A, et al. Frequency of mononuclear diploid cardiomyocytes underlies natural variation in heart

regeneration. *Nat Genet.* 2017;49(9):1346-53.

40. Lai ZF, Chen YZ, Feng LP, Meng XM, Ding JF, Wang LY, et al. Overexpression of TNNI3K, a cardiac-specific MAP kinase, promotes P19CL6-derived cardiac myogenesis and prevents myocardial infarction-induced injury. *Am J Physiol Heart Circ Physiol.* 2008;295(2):H708-16.

41. Vagnozzi RJ, Gatto GJ, Jr., Kallander LS, Hoffman NE, Mallilankaraman K, Ballard VL, et al. Inhibition of the cardiomyocyte-specific kinase TNNI3K limits oxidative stress, injury, and adverse remodeling in the ischemic heart. *Sci Transl Med.* 2013;5(207):207ra141.

42. Thorpe JA, and Schwarze SR. IRE1alpha controls cyclin A1 expression and promotes cell proliferation through XBP-1. *Cell Stress Chaperones.* 2010;15(5):497-508.

43. Romero-Ramirez L, Cao H, Nelson D, Hammond E, Lee AH, Yoshida H, et al. XBP1 is essential for survival under hypoxic conditions and is required for tumor growth. *Cancer Res.* 2004;64(17):5943-7.

44. Xu T, Yang L, Yan C, Wang X, Huang P, Zhao F, et al. The IRE1alpha-XBP1

pathway regulates metabolic stress-induced compensatory proliferation of pancreatic beta-cells. *Cell Res.* 2014;24(9):1137-40.

45. Iwakoshi NN, Lee AH, Vallabhajosyula P, Otipoby KL, Rajewsky K, and Glimcher LH. Plasma cell differentiation and the unfolded protein response intersect at the transcription factor XBP-1. *Nat Immunol.* 2003;4(4):321-9.

46. Casas-Tinto S, Zhang Y, Sanchez-Garcia J, Gomez-Velazquez M, Rincon-Limas DE, and Fernandez-Funez P. The ER stress factor XBP1s prevents amyloid-beta neurotoxicity. *Hum Mol Genet.* 2011;20(11):2144-60.

47. Wang ZV, Deng Y, Gao N, Pedrozo Z, Li DL, Morales CR, et al. Spliced X-box binding protein 1 couples the unfolded protein response to hexosamine biosynthetic pathway. *Cell.* 2014;156(6):1179-92.

48. Wettschureck N, Rutten H, Zywietz A, Gehring D, Wilkie TM, Chen J, et al. Absence of pressure overload induced myocardial hypertrophy after conditional inactivation of Galphaq/Galpha11 in cardiomyocytes. *Nat Med.* 2001;7(11):1236-40.

49. Clay H, Wilsbacher LD, Wilson SJ, Duong DN, McDonald M, Lam I, et al.

Sphingosine 1-phosphate receptor-1 in cardiomyocytes is required for normal cardiac development. *Dev Biol.* 2016;418(1):157-65.

Graphic Abstract

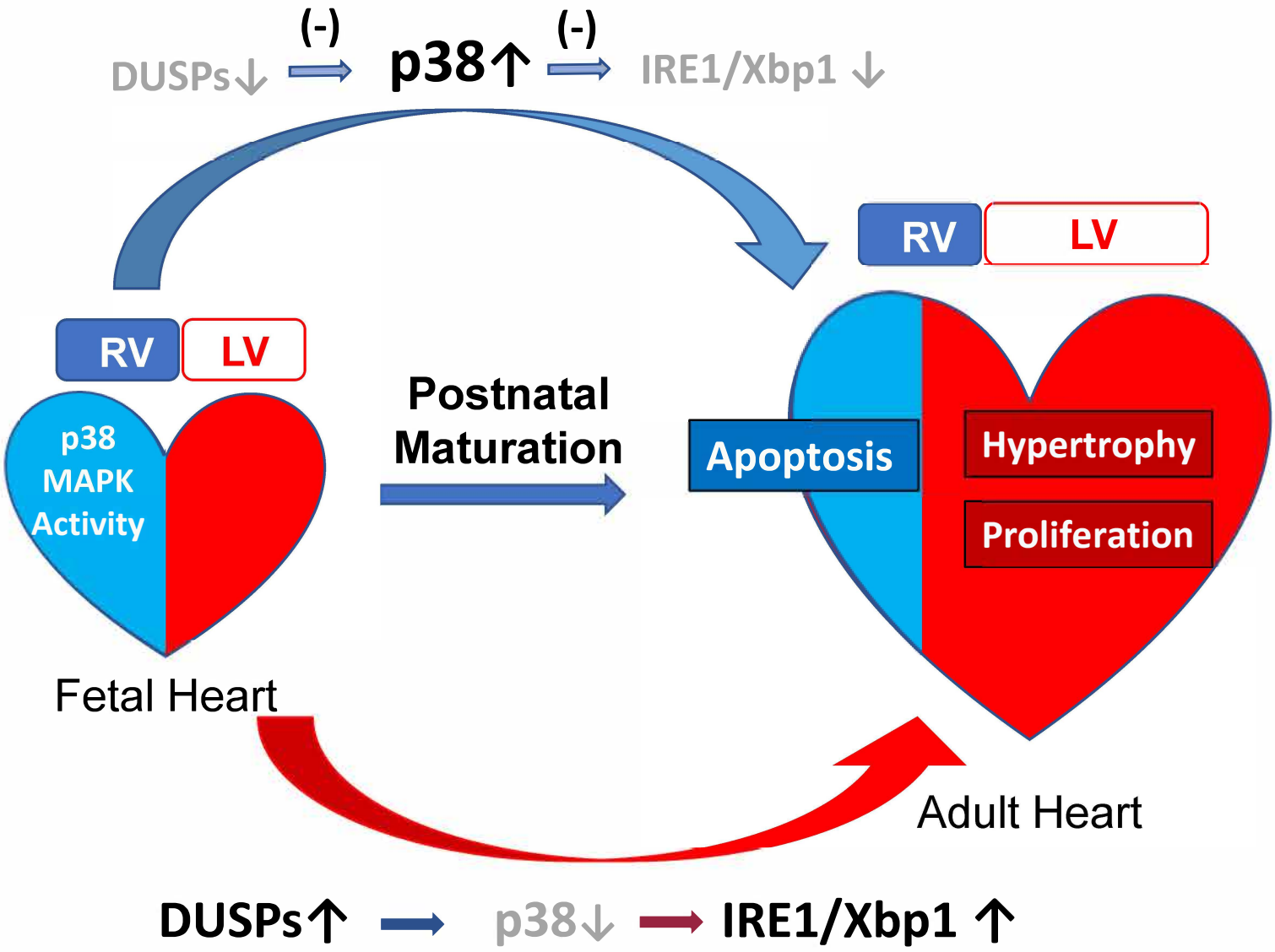

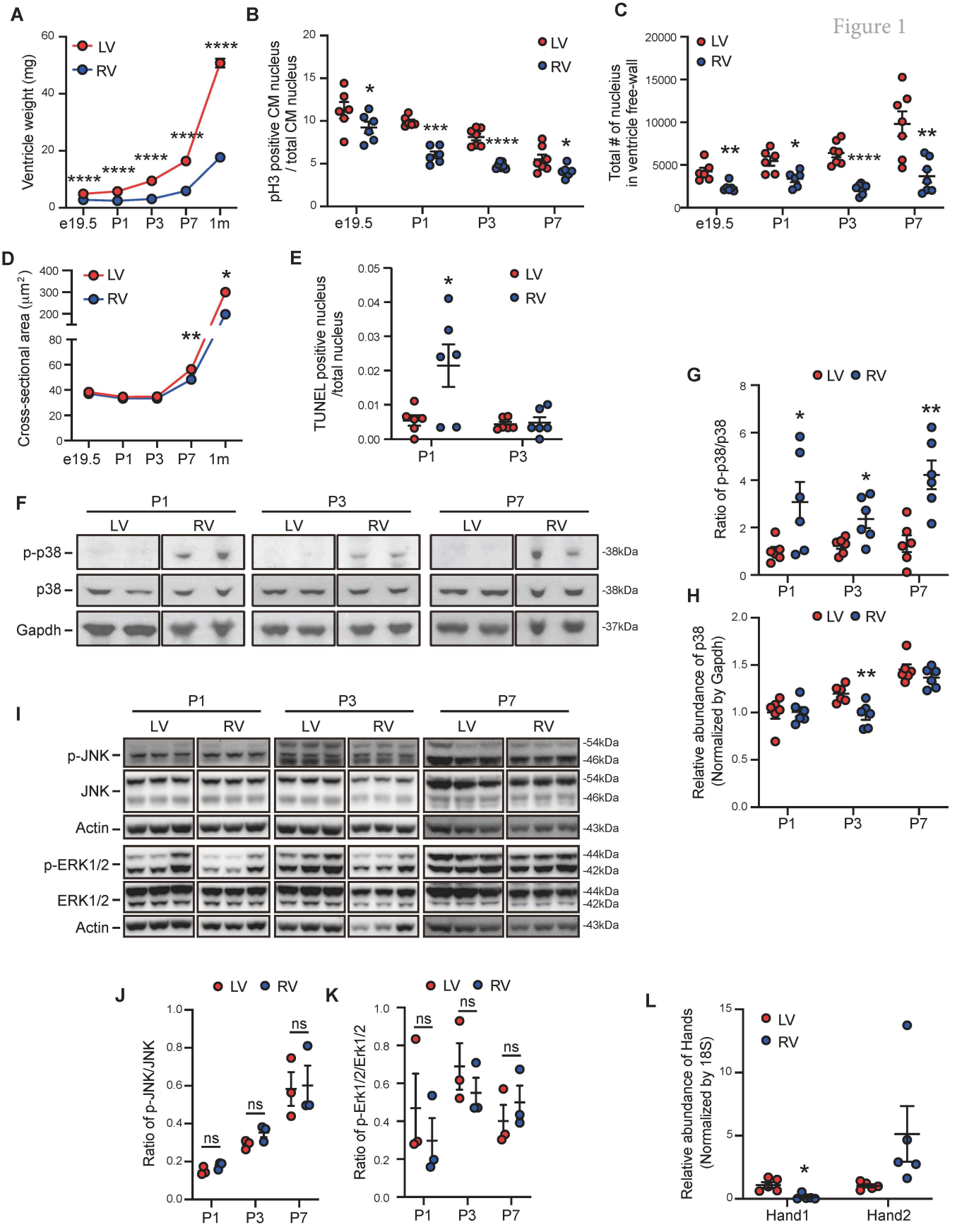
A
Ventricle weight (mg)
LV
RV
e19.5
P1
P3
P7
1m
B
pH3 positive CM nucleus / total CM nucleus
C
Total # of nucleus in ventricle free-wall
D
Cross-sectional area (μm²)
E
TUNEL positive nucleus /total nucleus
F
P1
P3
P7
p-p38
p38
Gapdh
-38kDa
-37kDa
G
Ratio of p-p38/p38
H
Relative abundance of p38 (Normalized by Gapdh)
I
p-JNK
JNK
Actin
p-ERK1/2
ERK1/2
-54kDa
-46kDa
-43kDa
-44kDa
-42kDa
J
Ratio of p-JNK/JNK
ns
K
Ratio of p-Erk1/2/Erk1/2
L
Relative abundance of Hands (Normalized by 18S)
Hand1
Hand2

Figure 1. Chamber-specific remodeling and activation of p38 MAP kinase during postnatal heart development. (A) The tissue weights of the left (LV) and the right (RV) ventricles of mouse perinatal heart at different timepoints as indicated (n=12, e19.5, n=16, P1, n=11, P3, n=9, P7, n=9, 1 month). **(B)** The number of phosphorylated-histone 3 (pH3) positive myocyte nuclei/total myocyte nuclei in LV vs. RV (n=6, e19.5, P1, n=7, P3, P7. **(C)** Total number of myocyte nuclei (n=6, e19.5, P1, n=7, P3, P7). **(D)** The cross-section area of myocytes (n=6, e19.5-P7, n=3, 1 month). **(E)** The number of TUNEL positive cardiomyocytes (n=6). **(F)** Representative immunoblots of phosph-p38, total p38 and Gapdh. **(G, H)** The ratio of phosphorylated p38 vs. total p38 signal (**G**) and total p38 (**H**) (n=6). (**I**) Representative immunoblots of phosphorylated ERK and JNK vs. total ERK and total JNK in mouse ventricles. **(J, K)** The ratio of phosphorylated JNK vs. total JNK signal (**J**) and phosphorylated ERK vs. total ERK signal (**K**) (n=3). **(L)** Chamber specificity of mRNA expression of Hand1 vs. Hand2 detected in the LV vs. RV free-wall prepared from P7 neonatal hearts (n=5). For all panels, mean ± SEM, RV vs. LV, *** $p<0.001$, ** $p<0.01$, * $p<0.05$.

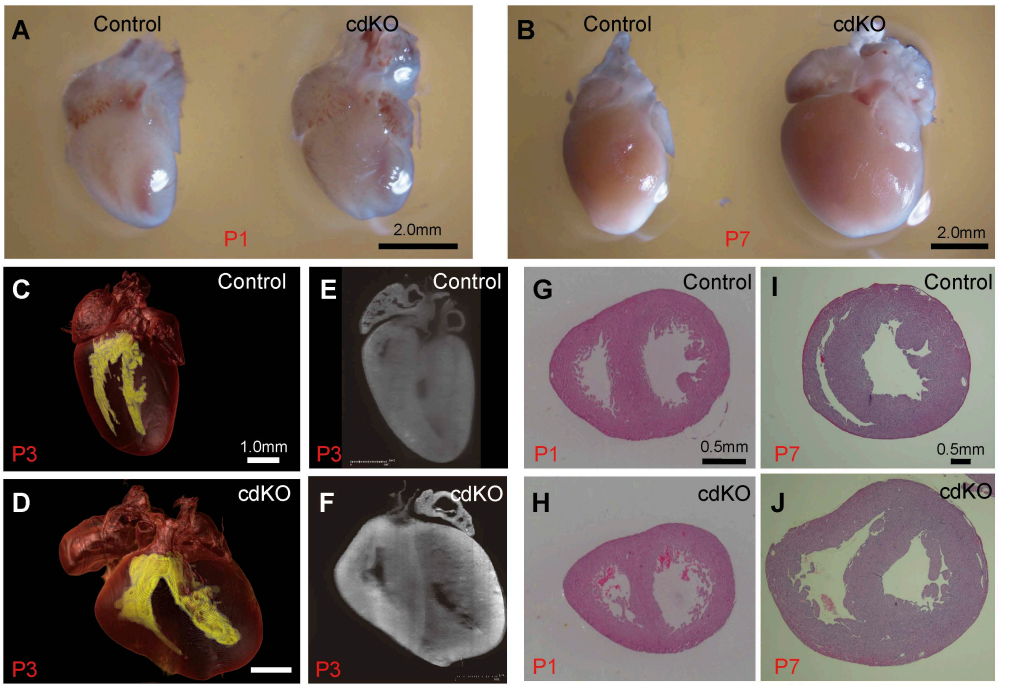
A
Control
cdKO
P1
2.0mm
B
Control
cdKO
P7
2.0mm
C
Control
P3
1.0mm
D
cdKO
P3
E
Control
P3
F
cdKO
P3
G
Control
P1
0.5mm
H
cdKO
P1
I
Control
P7
0.5mm
J
cdKO
P7

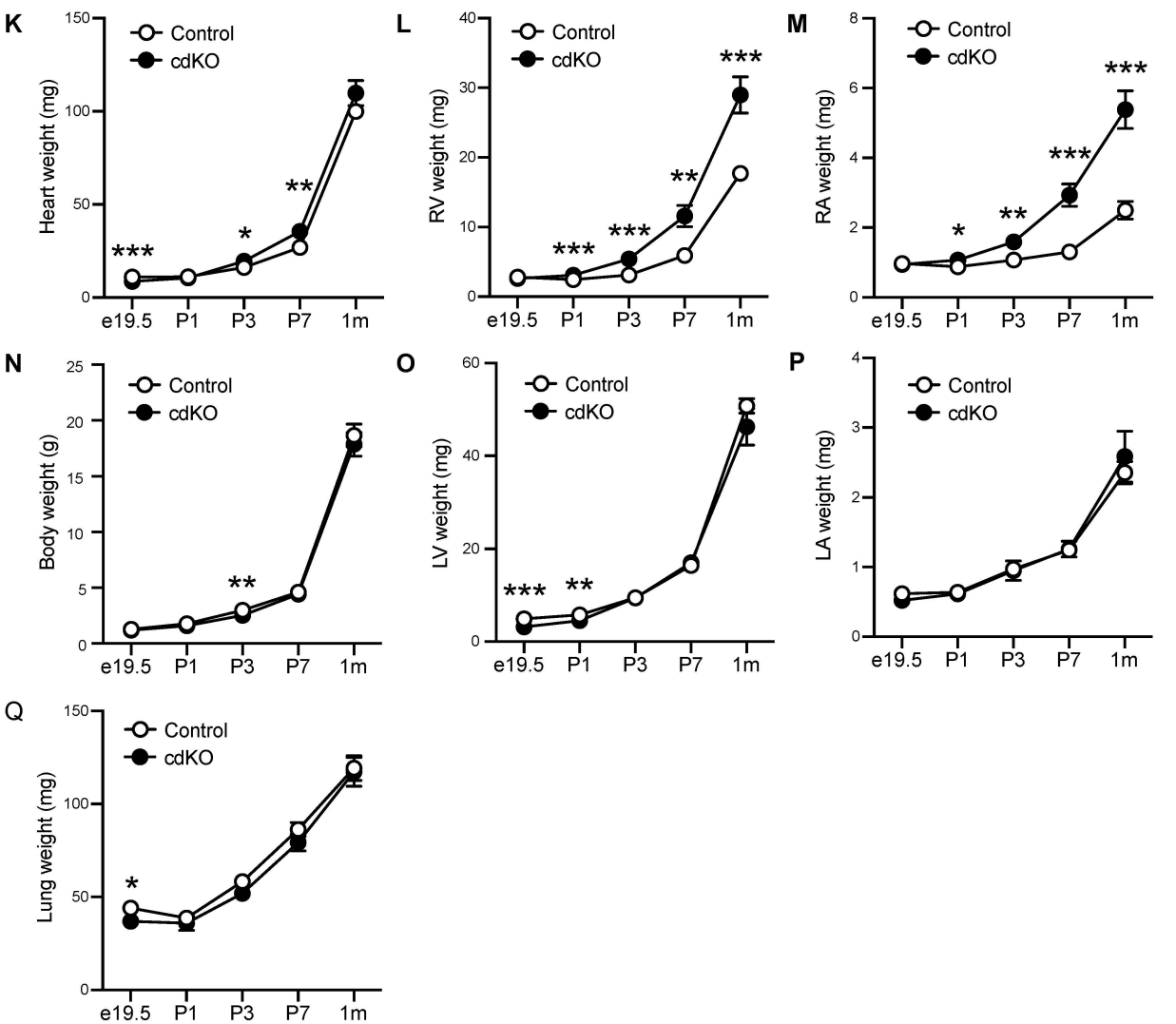
K
Heart weight (mg)
Control
cdKO
***
*
**
e19.5
P1
P3
P7
1m
L
RV weight (mg)
M
RA weight (mg)
N
Body weight (g)
O
LV weight (mg)
P
LA weight (mg)
Q
Lung weight (mg)

Figure 2. RV-specific abnormality in the cardiac-specific p38α/β MAP kinases knockout mouse. (A, B) Whole heart images of control and p38 cdKO at P1 **(A)** and P7 **(B)**. **(C-F)** Light-sheet imaging of whole heart from control (**C**) and p38cdKO (**D**) at P3. Inner cavity of ventricles is labeled in yellow. Sliced image from light-sheet imaging from Control (**E**) and p38cdKO (**F**) at P3. (**G, H**) H&E stained histological section of control heart (**G**) and p38cdKO heart (**H**) at P1. (**I, J**) H&E stained histological section of control heart (**I**) and p38cdKO heart (**J**) at P7. **(K-Q)** Weight measurements of whole heart (**K**), RV (**L**), RA (**M**), whole body (**N**), LV (**O**), LA (**P**), and lung (**Q**) in Control and p38cdKO mice during neonatal development (n=12 for e19.5, n=16 for P1, n=11 for P3, n=9 for P7, n=9 for 1 month, mean ± SEM). For all panels, *P* value (Control vs. cdKO) *** $p<0.001$, ** $p<0.01$, * $p<0.05$.

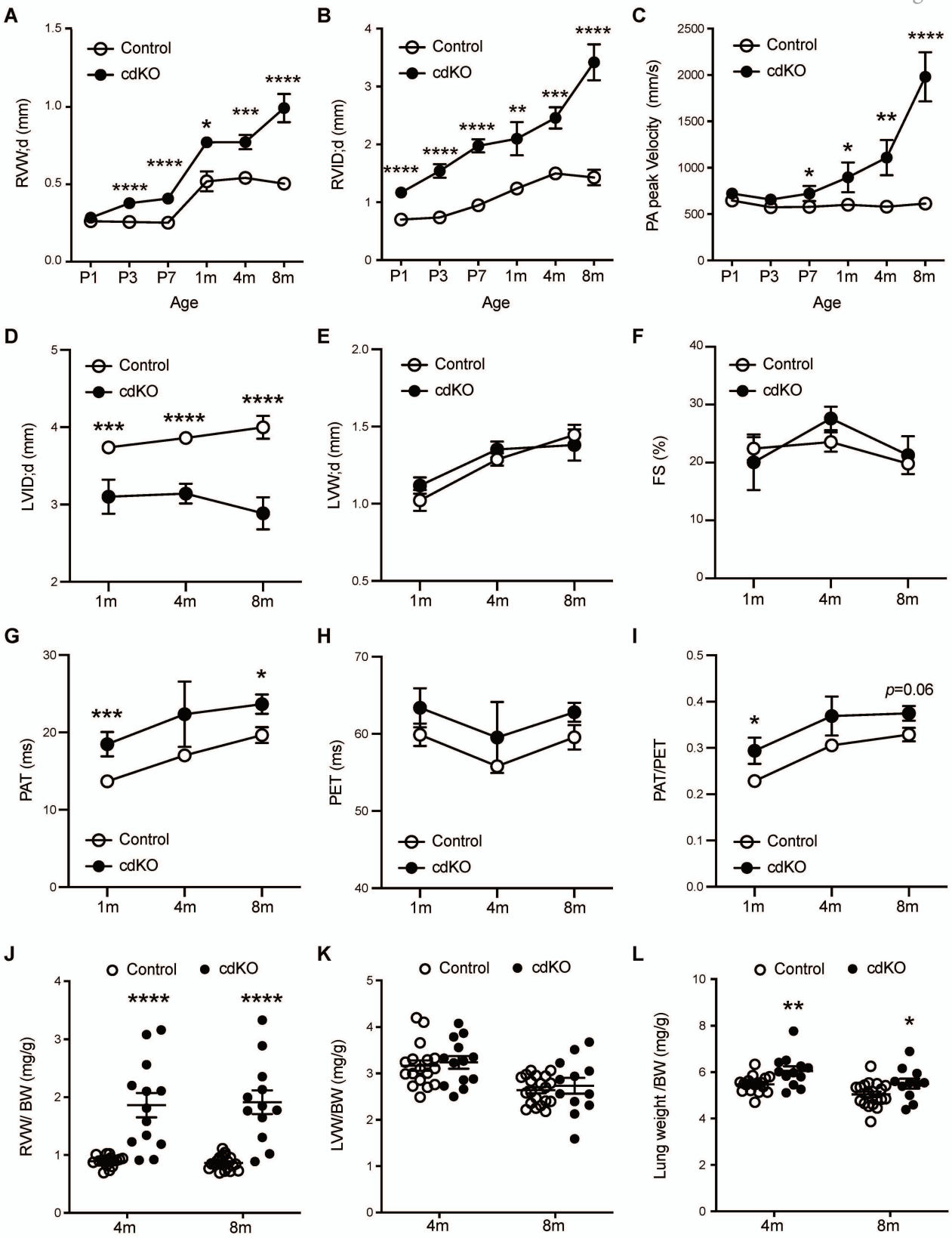
A
RVW;d (mm)
Control
cdKO
P1 P3 P7 1m 4m 8m
Age
B
RVID;d (mm)
C
PA peak Velocity (mm/s)
D
LVID;d (mm)
1m 4m 8m
E
LVW;d (mm)
F
FS (%)
G
PAT (ms)
H
PET (ms)
I
PAT/PET
p=0.06
J
RVW/ BW (mg/g)
4m 8m
K
LVW/BW (mg/g)
L
Lung weight /BW (mg/g)

Figure 3. Echocardiogram analysis showing RV specific abnormalities in the p38 cdKO mouse hearts. (**A-C**) Serial echocardiographic measurements in the Control and the p38cdKO mouse hearts for (**A**) end-diastolic RV wall thickness; (**B**) RV inner diameter; and (**C**) peak velocity at pulmonary artery in the Control and the p38 cdKO mice at different perinatal and postnatal time points as indicated. (Control n=16, cdKO n=12 at P1 (D1); Control n=17, cdKO n=12 at P3 (D3); Control n=20, cdKO n=10 at P7 (D7); Control n=8, cdKO n=5 at 1 month; Control n=11, cdKO n=7 at 4 months;Control n=10, cdKO n=6 at 8 months; mean± SEM). (**D-F**) LV echocardiogram parameters include **(D)** end-diastolic LV inner chamber diameter; **(E)** end-diastolic LV wall thickness; and **(F)** fractional shortening in the postnatal hearts. (Control n=8, cdKO n=5 at 1 month; Control n=14 cdKO n=10 at 4 months; Control n=10, cdKO n=6 at 8 months; mean ± SEM). (**G-I**) Pulmonary circulation indicators are: **(G)** pulmonary artery acceleration time; **(H)** PET; pulmonary ejection time; **(I)** PAT/PET ratio in the postnatal hearts. (Control n=8, cdKO n=5 at 1 month, Control n=14, cdKO n=10 at 4 months, Control n=10, cdKO n=6 at 8 months, mean ± SEM). (**J-L**) Ratio of RV free-wall (**J**), LV free-wall (**K**), and lung (**L**) weight to body weight at 4m and 8m. (Control n=17, cdKO

n=13 at 4 months; Control n=20, cdKO n=12 at 8 months, mean ± SEM). For all panels, p value (Control vs. cdKO) **** $p<0.0001$, *** $p<0.001$, ** $p<0.01$, * $p<0.05$.

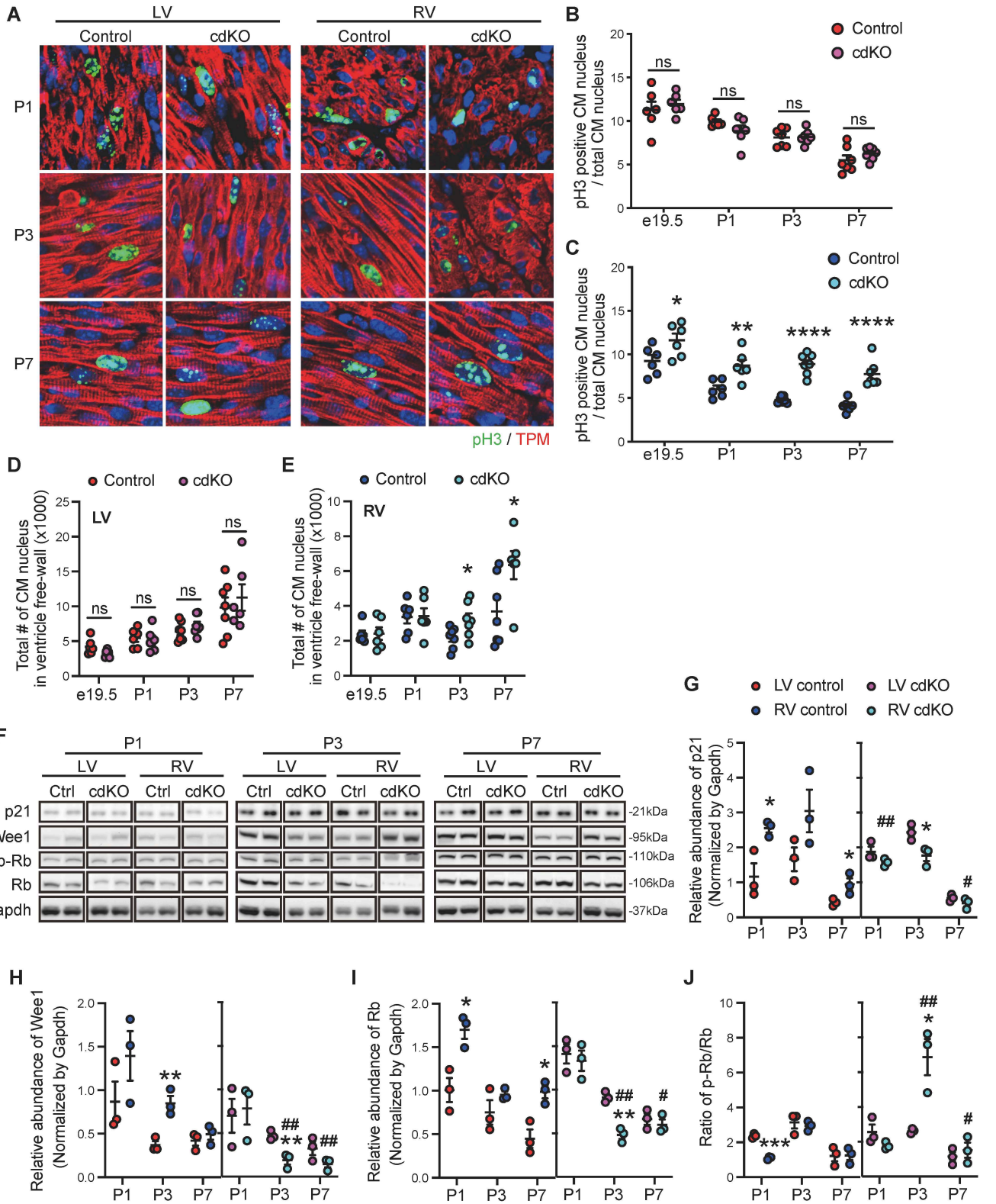
A
LV
RV
Control
cdKO
Control
cdKO
P1
P3
P7
pH3 / TPM
B
Control
cdKO
pH3 positive CM nucleus / total CM nucleus
ns
e19.5
P1
P3
P7
C
Control
cdKO
pH3 positive CM nucleus / total CM nucleus
*
**
****
****
e19.5
P1
P3
P7
D
Control
cdKO
LV
Total # of CM nucleus in ventricle free-wall (x1000)
ns
e19.5
P1
P3
P7
E
Control
cdKO
RV
Total # of CM nucleus in ventricle free-wall (x1000)
*
*
e19.5
P1
P3
P7
F
P1
P3
P7
LV
RV
Ctrl
cdKO
p21
Wee1
p-Rb
Rb
Gapdh
-21kDa
-95kDa
-110kDa
-106kDa
-37kDa
G
LV control
LV cdKO
RV control
RV cdKO
Relative abundance of p21 (Normalized by Gapdh)
P1
P3
P7
H
Relative abundance of Wee1 (Normalized by Gapdh)
I
Relative abundance of Rb (Normalized by Gapdh)
J
Ratio of p-Rb/Rb

Figure 4. RV-specific impact of p38 MAPK inactivation on myocyte proliferation in the neonatal heart. (A) Representative pictures of pH3/Tropomyosin staining of control and p38cdKO heart at P1, P3, and P7. **(B, C)** Quantification of pH3 positive myocyte nuclei/ total myocyte nuclei/section in the LV (**B**) and RV (**C**) from Control and cdKO during early postnatal development. (Control and cdKO n=6 at e19.5 and P1, n=7 at P3 and P7, mean ± SEM). (**D, E**) Total number of myocyte nuclei/section in the neonatal mouse in LV (**D**) and RV free-wall (**E**) from Control and cdKO at different time points. (Control and cdKO n=6 at e19.5 and P1, n=7 at P3, Control n=7 cdKO n=6 at P7, mean ± SEM). **(F-J)** Representative immunoblots (**F**) and quantification for protein expression of p21 (**G**), Wee1 (**H**), Rb (**I**), and pRb/Rb ratio (**J**). For all panels, p value (Control vs. cdKO) **** $p<0.0001$, *** $p<0.001$, ** $p<0.01$, * $p<0.05$.

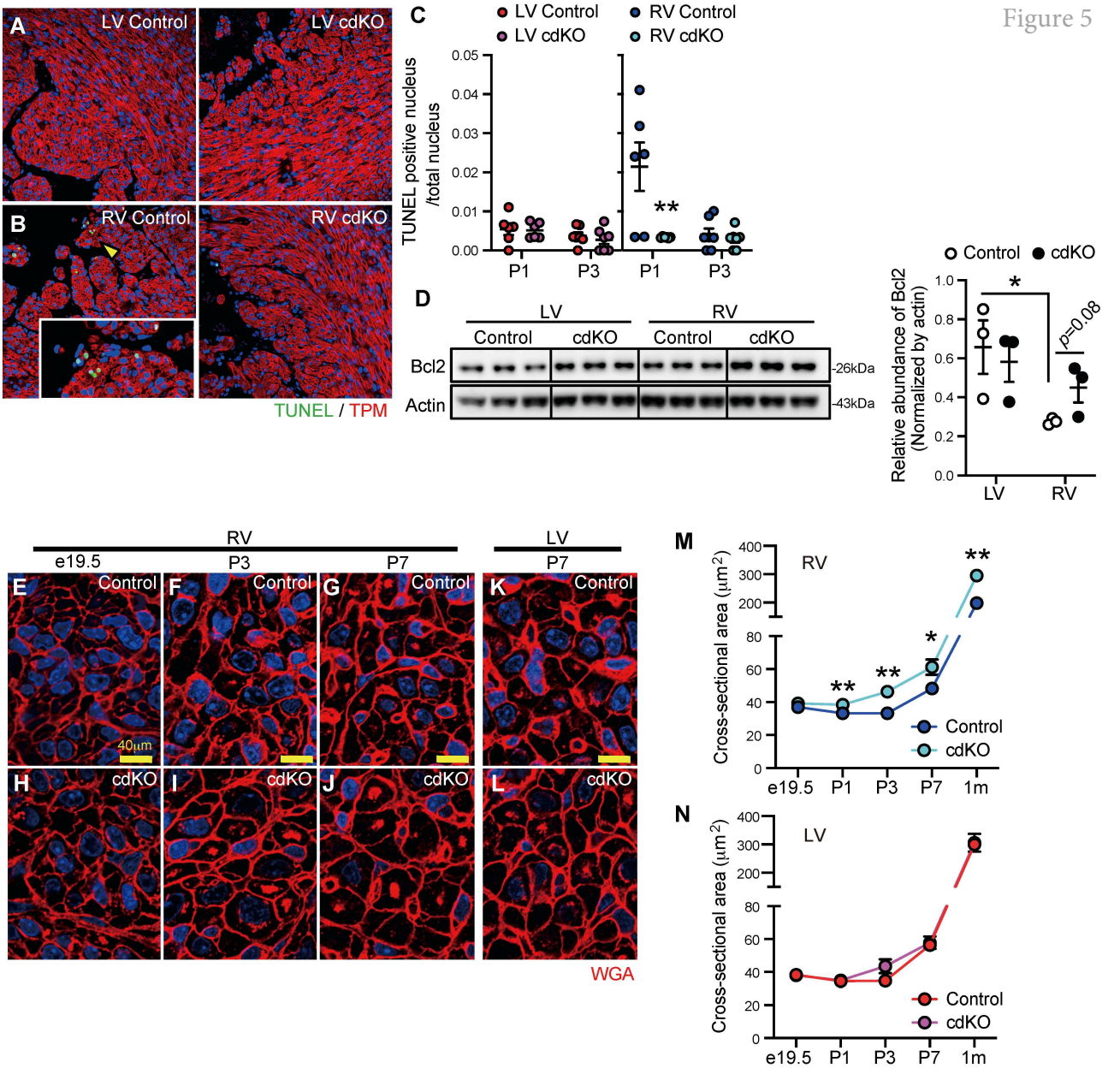
A
LV Control
LV cdKO
B
RV Control
RV cdKO
TUNEL / TPM
C
LV Control
LV cdKO
RV Control
RV cdKO
TUNEL positive nucleus /total nucleus
0.05
0.04
0.03
0.02
0.01
0.00
**
P1
P3
P1
P3
D
LV
RV
Control
cdKO
Control
cdKO
Bcl2
Actin
-26kDa
-43kDa
Control
cdKO
Relative abundance of Bcl2 (Normalized by actin)
1.0
0.8
0.6
0.4
0.2
0.0
*
p=0.08
LV
RV
RV
e19.5
P3
P7
LV
P7
E
Control
F
Control
G
Control
K
Control
40μm
H
cdKO
I
cdKO
J
cdKO
L
cdKO
WGA
M
RV
Cross-sectional area (μm2)
400
300
200
80
60
40
20
0
**
**
**
*
Control
cdKO
e19.5
P1
P3
P7
1m
N
LV
Cross-sectional area (μm2)
400
300
200
80
60
40
20
0
Control
cdKO
e19.5
P1
P3
P7
1m

Figure 5. RV-specific effects of p38 MAPK inactivation on cardiomyocyte death and hypertrophy. (A, B) Representative images of TUNEL staining in LV (**A**) and RV (**B)** with part labeled by arrowhead amplified in the insert) of the Control and p38 cdKO hearts at P1. (**C)** Percent TUNEL positive myocyte nuclei/total myocyte nuclei. (Control and cdKO n=6 at P1 and n=7 at P3, mean ± SEM). (**D**) Immunoblot and quantification of the Bcl2 protein level in the neonatal hearts at P1. (n=3. mean ± SEM). **(E-L)** Representative images of WGA staining in the RV from Control or p38cdKO hearts at E19.5 (**E, H**), P3 (**F, I**), and P7 (**G, J**) time points, and in the LV from Control or p38cdKO hearts at P7 (**K, L**). Scale bar indicates 40μm. **(M, N)** Cross-sectional area of myocytes from RV (**M**) and LV (**N**) during postnatal development. (Control and cdKO at 1 month n=3, other groups n=6, mean ± SEM). For all panels, P value (control vs. cdKO) ** $p<0.01$, * $p<0.05$.

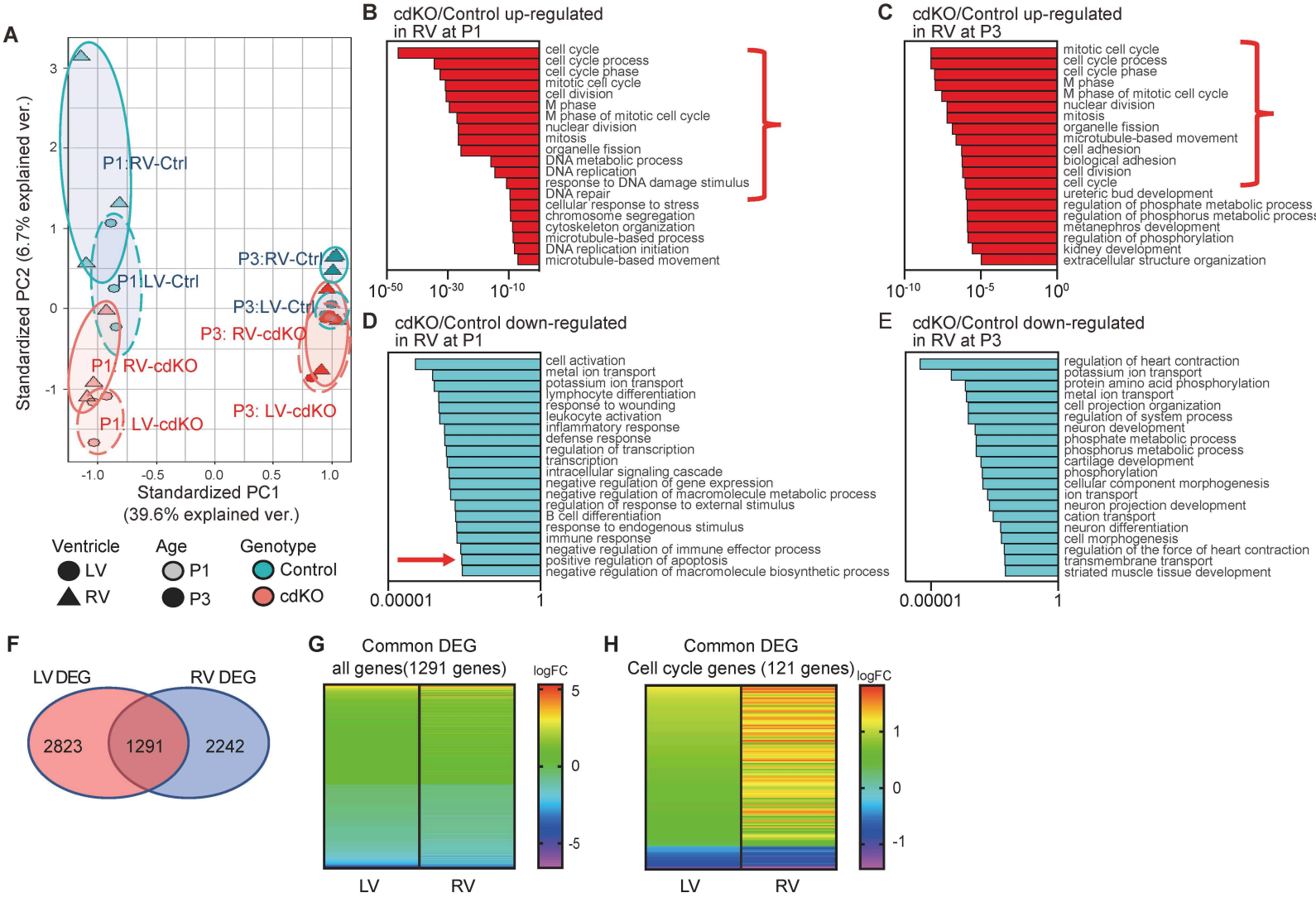
A
Standardized PC2 (6.7% explained ver.)
Standardized PC1
(39.6% explained ver.)
P1:RV-Ctrl
P1:LV-Ctrl
P3:RV-Ctrl
P3:LV-Ctrl
P3: RV-cdKO
P1: RV-cdKO
P3: LV-cdKO
P1: LV-cdKO
Ventricle
LV
RV
Age
P1
P3
Genotype
Control
cdKO
B
cdKO/Control up-regulated
in RV at P1
cell cycle
cell cycle process
cell cycle phase
mitotic cell cycle
cell division
M phase
M phase of mitotic cell cycle
nuclear division
mitosis
organelle fission
DNA metabolic process
DNA replication
response to DNA damage stimulus
DNA repair
cellular response to stress
chromosome segregation
cytoskeleton organization
microtubule-based process
DNA replication initiation
microtubule-based movement
C
cdKO/Control up-regulated
in RV at P3
mitotic cell cycle
cell cycle process
cell cycle phase
M phase
M phase of mitotic cell cycle
nuclear division
mitosis
organelle fission
microtubule-based movement
cell adhesion
biological adhesion
cell division
cell cycle
ureteric bud development
regulation of phosphate metabolic process
regulation of phosphorus metabolic process
metanephros development
regulation of phosphorylation
kidney development
extracellular structure organization
D
cdKO/Control down-regulated
in RV at P1
cell activation
metal ion transport
potassium ion transport
lymphocyte differentiation
response to wounding
leukocyte activation
inflammatory response
defense response
regulation of transcription
transcription
intracellular signaling cascade
negative regulation of gene expression
negative regulation of macromolecule metabolic process
regulation of response to external stimulus
B cell differentiation
response to endogenous stimulus
immune response
negative regulation of immune effector process
positive regulation of apoptosis
negative regulation of macromolecule biosynthetic process
E
cdKO/Control down-regulated
in RV at P3
regulation of heart contraction
potassium ion transport
protein amino acid phosphorylation
metal ion transport
cell projection organization
regulation of system process
neuron development
phosphate metabolic process
phosphorus metabolic process
cartilage development
phosphorylation
cellular component morphogenesis
ion transport
neuron projection development
cation transport
neuron differentiation
cell morphogenesis
regulation of the force of heart contraction
transmembrane transport
striated muscle tissue development
F
LV DEG
RV DEG
2823
1291
2242
G
Common DEG
all genes(1291 genes)
logFC
LV
RV
H
Common DEG
Cell cycle genes (121 genes)
logFC
LV
RV

Figure 6. Transcriptome changes in the p38cdKO heart. (**A**) Principal Component Analysis (PCA) of all expressed genes in the wildtype (WT, n=3) and p38cdKO (n=3) hearts at postnatal P1 and P3 time points from left (LV) and right (RV) ventricles. Circles represent PCA domains from each experimental group as labeled. (**B, C**) Gene Ontology (GO) classification of up-regulated genes in the p38cdKO RV comparing to Control at P1 (**B**) and P3 (**C**). **(D, E)** GO classification of down-regulated genes in the p38cdKO RV comparing to Control at P1 (**D**) and P3 (**E**). (**F**) A Venn diagram showing the overlap of differentially expressed genes (DEG) in cdKO between the LV and RV at P1 (n=3). (**G, H**) Heatmaps showing fold changes of the DEG shared by both ventricles at P1(n=1,291 genes) (**G**) and the cell cycle regulatory genes (n=121 genes) (**H**).

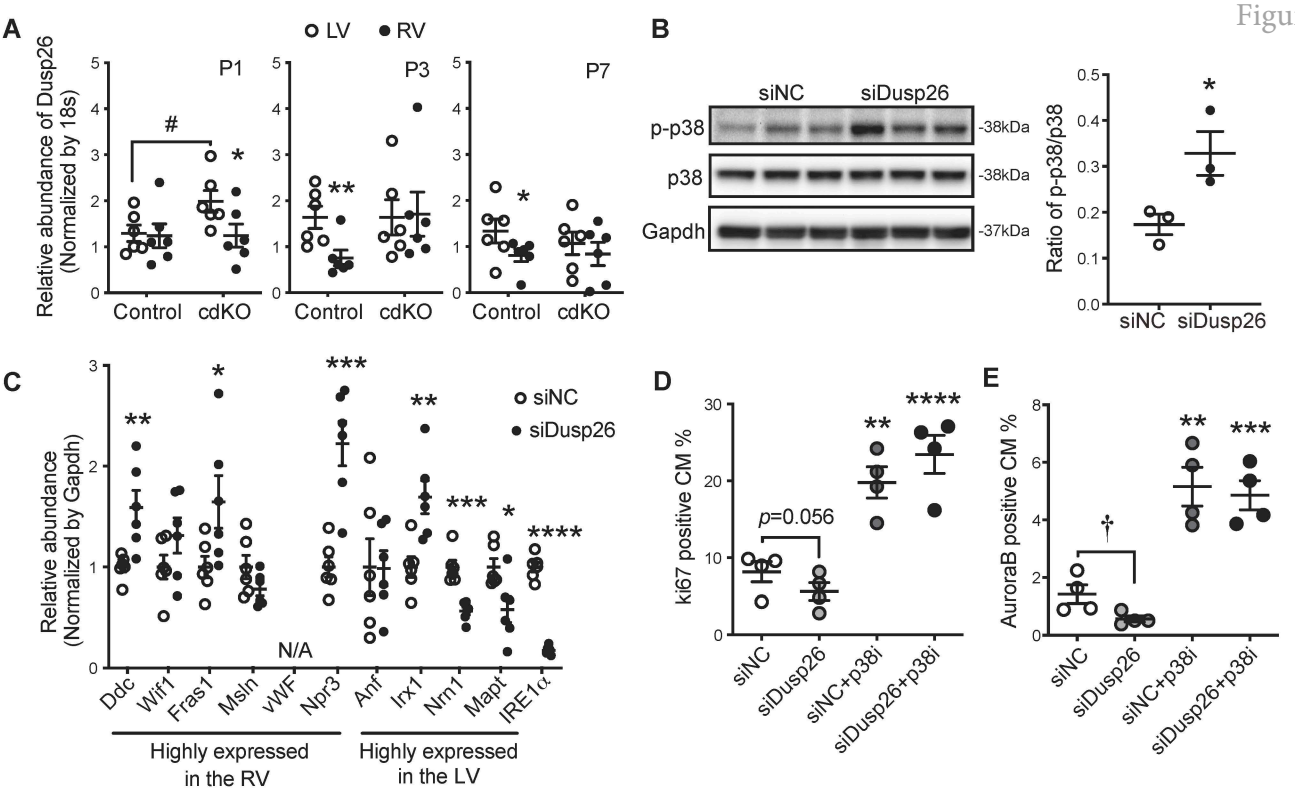
A
LV
RV
P1
P3
P7
Relative abundance of Dusp26 (Normalized by 18s)
Control
cdKO
B
siNC
siDusp26
p-p38
p38
Gapdh
-38kDa
-38kDa
-37kDa
Ratio of p-p38/p38
C
siNC
siDusp26
Relative abundance (Normalized by Gapdh)
N/A
Ddc
Wif1
Fras1
Msln
vWF
Npr3
Anf
Irx1
Nrn1
Mapt
IRE1α
Highly expressed in the RV
Highly expressed in the LV
D
ki67 positive CM %
p=0.056
siNC
siDusp26
siNC+p38i
siDusp26+p38i
E
AuroraB positive CM %
siNC
siDusp26
siNC+p38i
siDusp26+p38i

Figure 7. Dusp26 expression in chamber-specific p38 activation. (**A**) Chamber specific Dusp26 mRNA levels in the neonatal mouse heart at P1, P3 and P7 as indicated. (n=6. mean ± SEM) p value (LV vs. RV) ** $p<0.01$, * $p<0.05$. (Control vs. cdKO) # $p<0.05$. (**B**) p38 activation in cardiomyocyte treated with siRNA against Dusp26. (n=3. mean ± SEM). (**C**) mRNA expression of genes differentially expressed in each ventricle in the siDusp26 treated cardiomyocytes. (n=6. mean ± SEM). (**D**) The levels of ki67 or Aurora B positive cardiomyocytes following different treatments of p38 inhibition and Dusp26 inhibition. (n=4. mean ± SEM) P value (vs. siNC), **** $p<0.0001$, *** $p<0.001$,** $p<0.01$, * $p<0.05$.

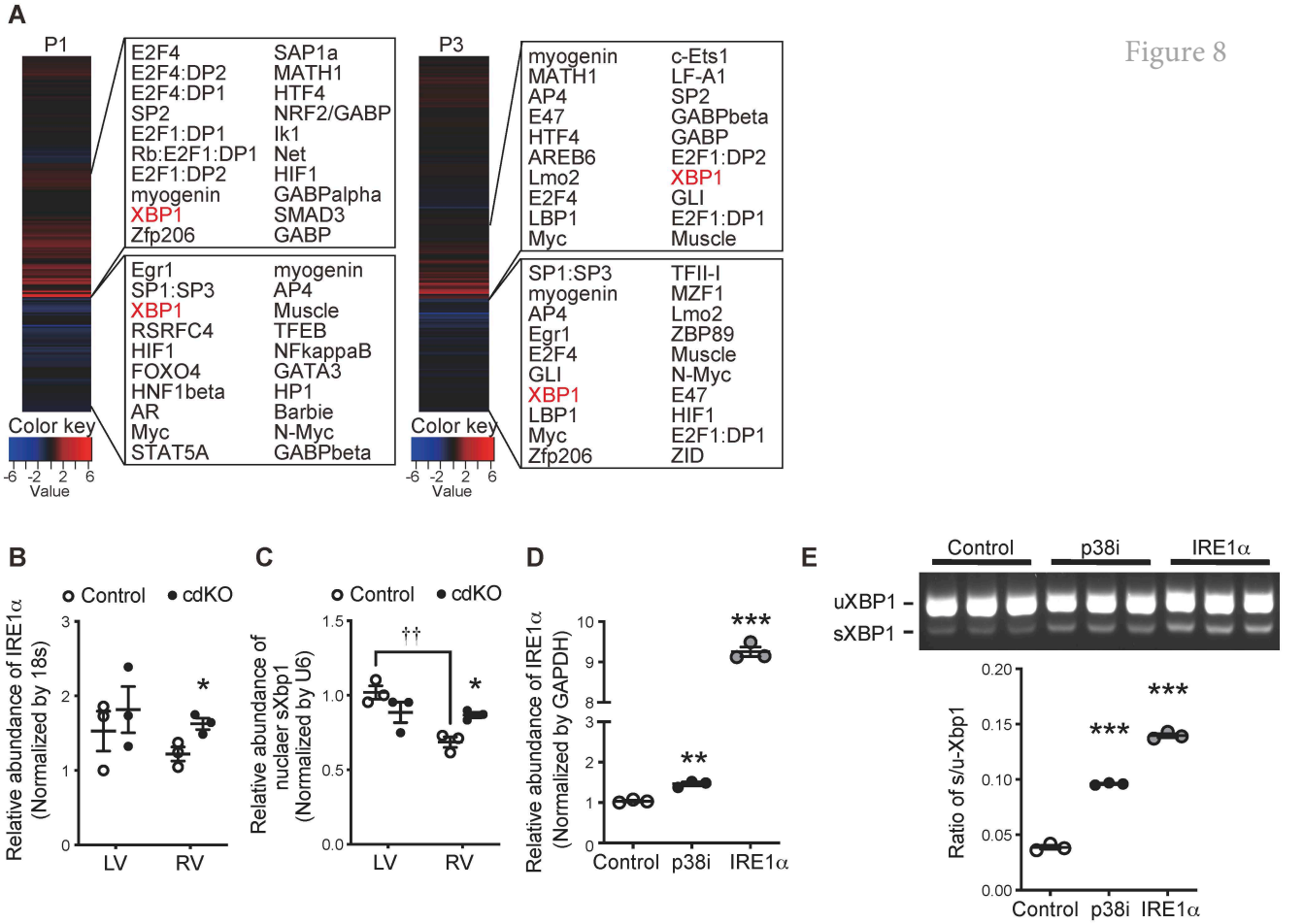
A
P1
E2F4
E2F4:DP2
E2F4:DP1
SP2
E2F1:DP1
Rb:E2F1:DP1
E2F1:DP2
myogenin
XBP1
Zfp206
SAP1a
MATH1
HTF4
NRF2/GABP
Ik1
Net
HIF1
GABPalpha
SMAD3
GABP
Egr1
SP1:SP3
XBP1
RSRFC4
HIF1
FOXO4
HNF1beta
AR
Myc
STAT5A
myogenin
AP4
Muscle
TFEB
NFkappaB
GATA3
HP1
Barbie
N-Myc
GABPbeta
Color key
-6 -2 2 6
Value
P3
myogenin
MATH1
AP4
E47
HTF4
AREB6
Lmo2
E2F4
LBP1
Myc
c-Ets1
LF-A1
SP2
GABPbeta
GABP
E2F1:DP2
XBP1
GLI
E2F1:DP1
Muscle
SP1:SP3
myogenin
AP4
Egr1
E2F4
GLI
XBP1
LBP1
Myc
Zfp206
TFII-I
MZF1
Lmo2
ZBP89
Muscle
N-Myc
E47
HIF1
E2F1:DP1
ZID
Color key
-6 -2 2 6
Value

B
Control
cdKO
Relative abundance of IRE1α (Normalized by 18s)
0
1
2
3
*
LV
RV

C
Control
cdKO
Relative abundance of nuclaer sXbp1 (Normalized by U6)
0.0
0.5
1.0
1.5
††
*
LV
RV

D
Relative abundance of IRE1α (Normalized by GAPDH)
0
1
2
3
8
9
10
**
***
Control
p38i
IRE1α

E
Control
p38i
IRE1α
uXBP1
sXBP1
Ratio of s/u-Xbp1
0.00
0.05
0.10
0.15
0.20
***
***
Control
p38i
IRE1α

Figure 8. IRE1α/Xbp1 and p38 MAPK activity in cardiomyocyte. (**A**) Whole genome-rVISTA analysis for the differential expressed genes in the P1 and P3 p38cdKO RV vs. the Control RV. The top 20 candidate transcription factors are listed for the upregulated genes (upper panels) and the down-regulated genes (bottom panels). **(B)** chamber specific expression of IRE1α mRNA in the P3 Control and the p38cdKO ventricles, (n=3. mean ± SEM). (**C**) Chamber specific expression of nuclear sXbp1 mRNA at P3 in the Control and the p38cdKO ventricles, (n=3. mean ± SEM). p value (Control vs. cdKO) * $p<0.05$. (LV vs. RV), # $p<0.05$. **(D)** IRE1α expression in the rat neonatal ventricular myocytes (NRVM) treated with p38i (SB202190) or Adv-IRE1α. (n=3. mean ± SEM) **(E)** The un-spliced (uXpb1) and spliced (sXbp1) Xbp1 levels in the NRVM treated with p38i (SB202190) or Adv-IRE1α. (n=3. mean ± SEM). p value (vs. Control) *** $p<0.001$, ** $p<0.01$.

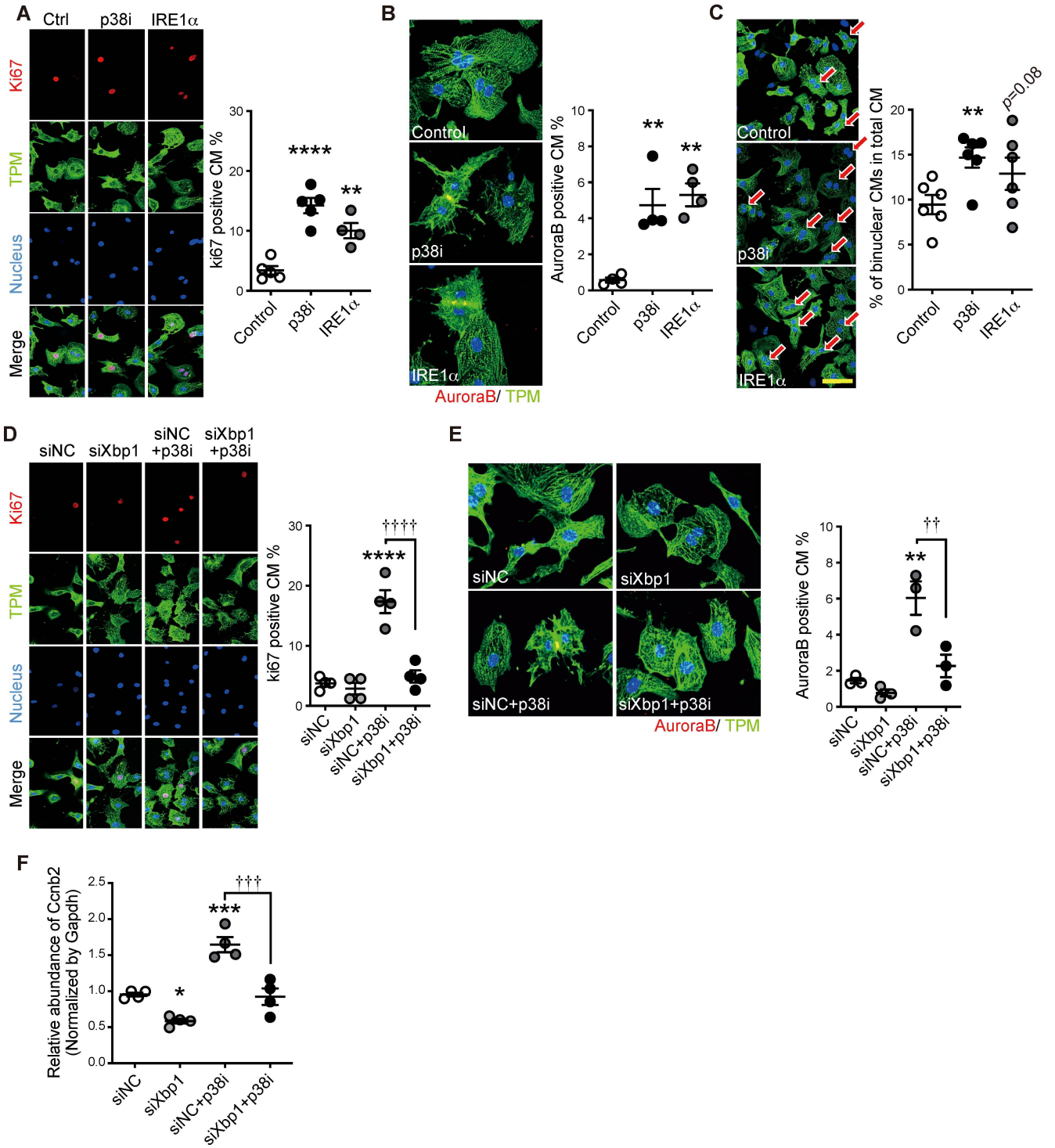
A
Ctrl
p38i
IRE1α
Ki67
TPM
Nucleus
Merge
ki67 positive CM %
Control
p38i
IRE1α
B
Control
p38i
IRE1α
AuroraB/ TPM
AuroraB positive CM %
C
% of binuclear CMs in total CM
p=0.08
D
siNC
siXbp1
siNC +p38i
siXbp1 +p38i
E
siNC
siXbp1
siNC+p38i
siXbp1+p38i
F
Relative abundance of Ccnb2 (Normalized by Gapdh)

Figure 9. IRE1α/Xbp1 and p38 MAPK activity in cardiomyocyte proliferation. (**A**) Representative immunohistochemical images and quantification of Ki67, (**B**) AuroraB positive, and (**C**) binucleated NRVM treated with p38i (SB202190) or Adv-IRE1α (n=4-6. mean± SEM). **(D)** Representative immunohistochemistry images/quantification of Ki67 and (**E**) AuroraB positive NRVM treated with p38i (SB202190) plus non-specific (siNC) or Xbp1 specific (siXbp1) silencing, (n=3-4. mean ± SEM). **(F)** mRNA levels of Ccnb2 (coding for Cyclin B2) in NRVM treated with p38i (SB202190) plus non-specific (siNC) or Xbp1 specific (siXbp1) gene silencing, (n=4. mean ± SEM). P value (vs. siNC) **** p<0.0001, *** p<0.001, ** indicates p<0.01, * p<0.05. (LV vs. RV, siNC+p38i vs. siXbp1+p38i) †††† p<0.0001, ††† p<0.001, †† p<0.01.